Available online at www.sciencedirect.com
SCIENCE DIRECT
Catalysis Today 113 (2006) 65–80
CATALYSIS TODAY
www.elsevier.com/locate/cattod

New frontier in transmission IR spectroscopy of molecules adsorbed on high surface area solids: Experiments below liquid nitrogen temperature

G. Spoto, S. Bordiga, A. Zecchina, D. Cocina, E.N. Gribov, L. Regli, E. Groppo, C. Lamberti *

Department of Inorganic, Physical and Materials Chemistry, NIS Centre of Excellence, University of Torino, Via P. Giuria 7, I-10125 Torino, Italy

Available online 4 January 2006

Abstract

IR spectroscopy of adsorbed probe molecules is one of the most powerful characterization techniques for the investigation of surface active sites on high surface area materials like oxides and zeolites. In the last 20 years the use of specific IR cells allowing the in situ sample activation, gas dosage and sample cooling down to liquid nitrogen temperature has remarkably improved the number and the quality of the information on the surface structure with respect to the first experiments carried out at room temperature. Commercial cryostats able to reach liquid helium temperatures are available since decades, but the incompatibility of the materials used to reach and confine very low temperatures with the high temperatures usually needed to activate the surfaces of catalysts has prevented for long time the breaking down of the 77 K frontier in IR experiments of species adsorbed on active surface sites. In our group we have very recently designed, realized and tested a new experimental set-up able to perform IR experiments in the 15–300 K interval on samples previously activated under vacuum conditions ($P < 10^{-4}$ Torr, 1 Torr $\sim$ 133.3 Pa), or in the desired atmosphere, up to 1073 K [G. Spoto, E.N. Gribov, G. Ricchiardi, A. Damin, D. Scarano, S. Bordiga, C. Lamberti, A. Zecchina, Prog. Surf. Sci. 76 (2004) 71]. The first results obtained with this innovative instrument will be reviewed and summarized in this work and compared with previous literature results on similar experiments performed at liquid nitrogen temperature. In particular, we will discuss the adsorption of CO and H_2 on MgO and H-SSZ-13 zeolite, and of H_2 on Cu^+-ZSM-5 zeolite.

Keywords: Transmission; Molecules; Temperature

1. Introduction

IR spectroscopy of adsorbed probe molecules has been widely employed in the characterization of active sites at the surface of heterogeneous catalysts [1–9]. In the last 20 years, the accurate control of the thermodynamic parameters involved in the experiment, like temperature (down to liquid nitrogen temperature), equilibrium pressure and contact time, allowed experimentalists on one side to remarkably improve the number and the quality of the information on the surface structure and, on the other hand, to alter the speed of the dynamic processes occurring on the surface, thus modifying the relative concentration of the precursor, intermediate and product species present at specific reaction conditions. In this context, time resolved (where temperature and pressure are kept constant during the experiment), temperature resolved (where the number of probe molecules in the cell is kept constant while changing the temperature) and pressure resolved (where temperature is fixed, while pressure is changing by acting on the number of probe molecules in the cell) FT-IR spectroscopy represents an useful tool for characterization purposes and for kinetic studies concerning several kind of reactions [10]. However, notwithstanding the fact that commercial cryostats able to reach liquid helium temperatures were available since decades and widely employed in the field of solid state physics [11–15], the lower temperature value at which experiments were performed was limited for a long period to 77 K, mainly due to practical problems. This was mainly due to the

* Corresponding author. Tel.: +39 011 6707841; fax: +39 011 6707855.
E-mail address: carlo.lamberti@unito.it (C. Lamberti).

0920-5861/$ – see front matter © 2005 Elsevier B.V. All rights reserved.
doi:10.1016/j.cattod.2005.11.011

incompatibility of the materials used to reach and confine very low temperatures with the high temperatures usually needed to activate the surfaces of catalysts, that has prevented for long time the overcoming of the 77 K barrier in FT-IR experiments of species adsorbed on active surface sites. Note that when speaking about 77 K IR experiments we mean a nominal temperature, being the actual one on the sample always slightly higher (typically in the 100–110 K range) owing to the temperature gradient between the cooled part of the cell and the sample itself and to the heating power of the IR beam.

The investigation of the vibrational features at surfaces at temperatures below that of liquid nitrogen has been performed since more than one decade by infrared reflection absorption spectroscopy (IRAS) [16–18] or by electron energy loss spectroscopy (EELS) [19–21]. Such investigations are however limited to vacuum-cleaved single crystal surfaces or to thin (few monolayers thick) oxide films epitaxially grown on metal substrates, i.e. on systems that are often far away from real catalysts. The 77 K frontier in FT-IR adsorption experiments on high surface area powdered materials has been broken down very recently, thanks to the realization in our laboratory of an unique experimental set-up able to perform FT-IR experiments in transmission mode down to 15 K on materials activated in situ under vacuum conditions ($P < 10^{-4}$ Torr) and at temperatures up to 1100 K [22]. In this work we summarize and review the first results obtained with this innovative instrument, demonstrating that this experimental strategy has a very high sensitivity.

Lowering the temperature allows some relevant improvements. The usually adopted probe molecules for IR spectroscopy (CO, NO, Py, etc.) often interact strongly with the surface sites, resulting in a significant perturbation of the site itself upon molecule adsorption. The ideal probe molecule for a given site should, consequently, be characterized by an as low as possible adsorption enthalpy (ΔH). However, as the equilibrium between molecules in the gas phase and in the adsorbed state is driven by the Gibbs function ($\Delta G = \Delta H - T\Delta S$), and as adsorbed states requires a relevant decrease of the entropy of the system, a significant fraction of molecules in the adsorbed state can be obtained only once the entropic term is minimized by suitably low temperatures. As a consequence, to observe an adsorption process characterized by a given adsorption enthalpy of ΔH, the experiments should be performed at temperature T in the order of $\Delta H/\Delta S$ or lower. On the other side, adsorption measurements performed at a given temperature T are able to monitor processes characterized by a ΔH value in the order of $T\Delta S$ or higher.

Among the molecules able to slightly perturb the surface site we can mention N_2 and H_2. These molecules (particularly H_2) have been scarcely employed up to now in the surface characterization because even temperatures in the range of that of liquid nitrogen are not sufficiently low to reduce the entropic term in a significant way for most of the surface sites. The possibility to use H_2 as probe molecule for surface characterization is particularly attractive as, owing to the presence of a single bond (H–H), the H–H stretching is expected to undergo a much higher $\Delta\tilde{\nu}_{HH}$ shift than that underwent by the C≡O or the N≡O stretching, when CO or NO molecules are adsorbed on the same site. This open new prospects in the discrimination among rather similar surface sites.

For these reasons, the experiments carried out in the 15–300 K temperature interval can be of extreme utility for complementing the experimental information on the surface structure obtained with similar experiments performed at liquid nitrogen temperature. Finally, it will be shown that this experimental set-up allows to perform experiments by controlling both the equilibrium pressure of the probe molecule and the adsorption temperature, so that new site-specific thermodynamic data can be obtained that could not be obtained before by classical calorimetric experiments, where integrated (on all adsorption sites) values are accessed.

In particular, in this contribution the results concerning three main topics will be discussed: the adsorption of CO and of H_2 on MgO surfaces and on H-SSZ-13 zeolite and the H_2 adsorption on Cu^+-ZSM-5 zeolite. We will show that the new experimental set-up allowed to add new information on the interaction of the CO and H_2 probes with the surface cations and anions on the MgO samples, so that a much more complete view on the topic has been reached. In particular, the investigation of CO olygomerization on MgO conducted at 60 K gave the opportunity of studying monomeric and oligomeric precursors of the polymeric species formed at higher temperatures on the low coordinated O^{2-} sites present at the MgO surface, while experiments conducted at 20 K allowed to observe for the first time some transient molecularly adsorbed H_2 precursor of hydride and hydroxyl species formed on the Mg^{2+} cations. Finally, experiments at 15 K allowed to identify two distinct $Cu^+(H_2)$ adducts formed inside Cu^+-ZSM-5 zeolite and to follow their evolution upon changing the H_2 pressure. As for H-SSZ-13 zeolite, the new low temperature IR experiments allowed to define the correct acidic proton distribution among the four crystallographic independent ones.

2. Experimental

2.1. Materials and procedures

2.1.1. MgO samples

The new advances presented in this work refer to two different MgO polycrystalline samples characterized by significant different surface areas: ∼230 and ∼40 $m^2\,g^{-1}$, hereafter high surface area (hsa) and sintered MgO samples, respectively. The hsa sample was obtained by decomposition of $Mg(OH)_2$ in vacuo, while the sintered sample was obtained from the hsa one by prolonged sintering at 1073 K according to the well known procedure described in Refs. [5,9,23–26]. Before the experiments, all of the samples were pressed into pellets suitable for transmission IR measurements. More details on the sample preparation have been reported elsewhere [22].

It is widely accepted that on hsa MgO the concentration of surface defects (edges, steps, and corners) reaches a maximum, and this explains the complexity of the IR spectra of adsorbed CO (vide infra Section 3.1) and of dissociatively adsorbed

hydrogen (vide infra Section 3.2) published so far and the difficulties encountered in the vibrational assignments. Conversely, by progressively sintering the hsa MgO sample under controlled temperature conditions (obtaining the sintered MgO), it is possible to gradually decrease in a controlled way the defects concentration, thus decreasing the number of the surface species formed by adsorption and hence simplifying the IR spectra.

2.1.2. Cu^+-ZSM-5 sample

Cu^+-ZSM-5 was prepared by reaction of H-ZSM-5 (Si/Al ~ 90) with gaseous CuCl, according to the reaction path: $Si(OH^+)Al_{(surf)}^- + CuCl_{(g)} \rightarrow Si(OCu^+)Al_{(surf)}^- + HCl_{(g)}$. This procedure leads to a 1:1 substitution of the zeolite acidic protons exclusively with isolated Cu^+ ions (i.e. to a very well defined system from the point of view of the copper ions' local environment). Cu^+-ZSM-5 samples prepared following our method have been of great help in understanding the local structure of Cu^+ ions in zeolites that certainly affects their catalytic behavior. In fact, because of its model character, the system offers clear and simple spectroscopic, energetic and structural outputs which assignment is straightforward [27–40]. This is the reason why the experimental results emerging from its characterization have been also used as model values for comparison of the computational outputs obtained in advanced quantum chemical studies [41–48].

2.1.3. H-SSZ-13 sample

Zeolite SSZ-13 was synthesized at the Chemistry Department of the Oslo University (Bjørgen and Lillerud) by following a hydrothermal preparation procedure described in the patent by Zones [49]. A carefully controlled calcination procedure, aiming at preserving the crystallinity of the material, has been adopted. The template removal was carried out in a pure oxygen flow (20 ml/min) in a fixed bed tubular quartz reactor according to the following procedure: the as-synthesized sample was initially heated to 573 K and left at this temperature for 12 h. The temperature was slowly increased to 773 K and kept isothermal for another 12 h. Powder XRD confirmed a pure SSZ-13 phase. Qualitative elemental analysis and sample morphology were examined using a Philips XL 30 Scanning Electron Microscope. The Si/Al ratio was 11.6 and average particle size was in the range 5–10 μm. Surface area has been obtained by means of N_2 adsorption performed at 77 K. The volumetric measurements have been performed with a Micromeritics ASAP 2010 sorption analyzer. From the N_2 adsorption data, BET area of 638 $m^2\ g^{-1}$, Langmuir area of 843 $m^2\ g^{-1}$ and micropore volume of 0.277 ml g^{-1} (from the *t*-plot) have been obtained [50,51].

2.2. Low temperature IR instrument

The infrared spectroscopic measurements were performed using a properly designed cryogenic cell allowing the in situ high-temperature activation (up to 1073 K) of the sample under vacuum condition (or in desired atmosphere). The instrument allows to monitor the modification of the IR spectra of molecules adsorbed on clean surfaces according to two main procedures. The first one consists in adsorption experiments at fixed temperature (down to 15 K, estimated at the sample level), and variable equilibrium pressure of the probe molecule. The second procedure concerns the recording of the IR spectra of the species adsorbed in the whole temperature interval (from 300 to 15 K) while simultaneously measuring the gas phase equilibrium pressure. By this procedure it is possible to measure the integrated area of a specific IR band upon changing the sample temperature, which in turn allows to calculate the site-specific adsorption enthalpy of the corresponding surface adduct. In both procedures, time invariance of the spectra has been used as a criterium to prove that the system has reached the equilibrium at the given thermodynamic condition (pressure and temperature).

A detailed description of the cryogenic cell (consisting of a properly modified closed circuit liquid helium Oxford CCC 1204 cryostat) is given elsewhere [22]. The spectra were acquired at a resolution of 1 cm^{-1} on a Bruker Equinox-55 FT-IR spectrometer whose sample compartment was modified ad hoc to accommodate the cryogenic IR cell. All of the spectra reported in the following are background subtracted using the spectrum of the pure MgO, Cu^+-ZSM-5 or H-SSZ-13 as reference (with the only exception of Fig. 9a and c).

3. Results and discussion

3.1. CO adsorption and olygomerization on high surface area MgO surface: FT-IR experiments at 60 K

Carbon monoxide has been historically one of the most used probe in the investigation of the MgO surface. Basically, the properties of the CO/MgO system can be discussed in terms of: (i) species formed by interaction of CO with the positive Mg^{2+} surface centers and (ii) species formed on the low coordinated O^{2-} centers. In the following, we will highlight the improvements in the characterization of both these species obtained by performing FT-IR experiments at 60 K. We will show that a decrease of about 40 K with respect to the classical IR experiments reported in the literature resulted in a remarkably detailed evolution of the spectra as a function of CO pressure, allowing to better understand the complex interaction of the CO molecule with the different cationic and anionic sites of the MgO surface. The attention will be mainly focused on the results obtained on hsa MgO samples, but reference to sintered material will be also done for comparison.

3.1.1. CO adsorption on Mg^{2+} sites

Mg_{3c}^{2+}(CO) adducts, formed by interaction of CO with Mg_{3c}^{2+} located at corner sites, are clearly observed in the IR spectrum of CO adsorbed at RT, already reported in early studies [24,52,53]. Experiments performed at about 100 K showed that CO is able to distinguish among surface Mg^{2+} sites of different coordinative unsaturation [5,9,23–26,52,54–57]. In particular, at very low coverage ($\theta < 0.1$) the frequency of CO (singleton) adsorbed through the carbon end on Mg_{3c}^{2+}, Mg_{4c}^{2+}, and Mg_{5c}^{2+}, is upward shifted with respect to the frequency of the CO gas of +60, +27 and +14 cm^{-1},

respectively ($\tilde{\nu}$(CO) = 2203, 2170 and 2157 cm^{-1}). This shift is the typical result of the Stark effect associated with the positive electric field of the cation. Following Hush and Williams [58] and Pacchioni et al. [59], when no d-electrons are involved, the shift is, for moderate fields, proportional to the strength of the electric field sensed by CO. The stability of the Mg^{2+}(CO) species is in the order: corners $Mg_{3c}{}^{2+}$(CO) > steps and edges $Mg_{4c}{}^{2+}$(CO) > (1 0 0) faces and terraces $Mg_{5c}{}^{2+}$(CO).

On the basis of all these results it is concluded that, by using appropriate pressure and temperature conditions, CO selectively probes the vast majority of the positive centers of the MgO surface and hence gives comprehensive information on the structure and distribution of the Mg^{2+} centers. However, it is worth to underline that despite the extensive work carried out in this field, not all of the numerous species formed by interaction of CO with positive centers have been unambiguously assigned so far. In order to obtain a more complete description of the Mg^{2+}(CO) species formed on the MgO surface, Spoto et al. [22] have recently performed CO adsorption experiments by lowering the sample temperature down to 60 K, thus appreciating new fine spectroscopic details which escaped detection in the previous works.

FT-IR spectra of CO dosed at 60 K on hsa and sintered MgO samples are shown in the CO stretching region in Fig. 1a and b, respectively. The most intense spectra of the two sequences correspond to P_{CO} = 40 Torr. The other spectra have been obtained by decreasing the pressure in steps at constant T of 60 K. The spectra with lowest intensity have been obtained after prolonged pumping at 60 K and correspond to CO equilibrium pressures lower than 10^{-3} Torr. The two sequences reported in Fig. 1 allow us to appreciate directly how the decrease of the specific surface area is accompanied by a dramatic decrease of intensity and by a drastic spectral simplification.

Considering the high frequency region of the spectra, the weak band at 2205–2200 cm^{-1} was already assigned to $Mg_{3c}{}^{2+}$(CO) complexes [9,59,60]. This assignment well explains why this band is well evident in the case of hsa material but very weak on sintered sample. However, the high quality of the spectra on hsa sample allowed Spoto et al. [22] to observe a distinct tail on the low frequency side of this band, which has been explained on the basis of the presence of many surface configurations containing three-fold coordinated ions, differing in the second coordination sphere. Upon increasing the P_{CO} the peak observed at 2203 cm^{-1} first increases, than it saturates and finally disappears with formation of a shoulder at about 2185 cm^{-1}. This fact is well known and has been attributed to the evolution from monocarbonylic to dicarbonylic species [22,61]. At higher pressures, also the shoulder at 2185 cm^{-1} gradually disappears, plausibly because the responsible peak is shifting to lower frequency and becomes obscured by the extremely strong bands associated with the more abundant $Mg_{4c}{}^{2+}$(CO) and $Mg_{5c}{}^{2+}$(CO) complexes. This shift could be associated with formation of tricarbonylic species [22].

By increasing P_{CO}, after formation of $Mg_{3c}{}^{2+}$(CO) adducts at three-fold sites, also $Mg_{4c}{}^{2+}$ sites begin to be populated and two new strong and complex absorptions in the 2180–2160 and 2150–2145 cm^{-1} intervals appear on both the hsa and sintered samples. These absorptions have a composite character, easily explained with the heterogeneity of the $Mg_{4c}{}^{2+}$ sites (located on

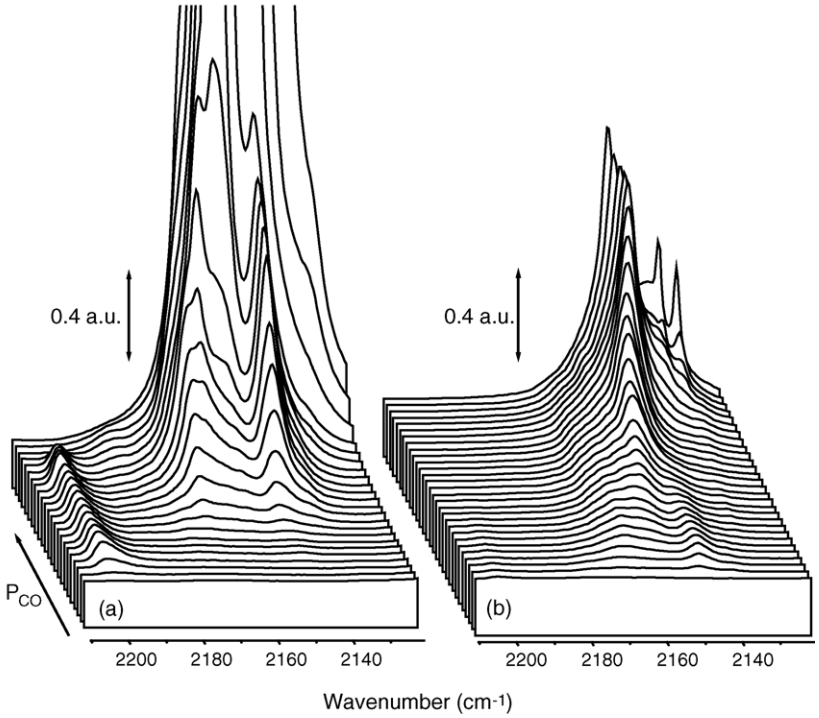

Fig. 1. Pressure dependance of the FT-IR spectra, in the CO stretching region, of CO dosed at 60 K on hsa and sintered MgO samples, part (a) and (b), respectively. Increasing CO pressure from front to back spectra. Adapted from Ref. [22], with permission. Copyright (2004) by Elsevier.

edges and steps of variable height). On both hsa and sintered materials the intensity of these peaks is at least one order of magnitude higher than that of the Mg_{3c}^{2+}(CO) species. Finally, the narrow and dominant peak observed on sintered MgO in the 2157–2149 cm^{-1} interval was attributed to the ν(CO) mode of molecules perpendicularly adsorbed through the carbon end on five-fold coordinated Mg^{2+} ions of (1 0 0) terraces and facelets. On hsa material the evolution of this peak upon the CO pressure cannot be clearly observed; in fact, at high θ its intensity is exceedingly high, while at low θ it is superimposed to the bands of CO interacting with Mg^{2+} sites exhibiting a higher coordinative unsaturation, as discussed above.

Till now we have discussed the effect of changing the gas pressure on the IR spectra of the MgO/CO system collected at constant T (60 K). By the same experimental apparatus used for this kind of experiment it was also possible to collect the spectra by working at constant equilibrium pressure while gradually changing the temperature in the whole RT−60 K range. Spoto et al. [22] performed such isobaric experiment (P_{CO} = 60 Torr) on the MgO/CO system in the 300–60 K interval. The intensity of the bands (hereafter A) at 2150 and 2170 cm^{-1}, ascribed to the Mg_{4c}^{2+}(CO) complexes, and of the band at ∼2157 cm^{-1}, ascribed to Mg_{5c}^{2+}(CO) complexes (vide supra), was so measured as a function of T. For both bands, the intensities increase gradually upon decreasing T and asymptotically reaching a maximum (A_{max}) at different T, corresponding to saturation conditions. The ratio between the intensity measured at a given T ($A(T)$) and that at saturation conditions (A_{max}) allows to quantitatively know the fraction of sites covered by CO, defined as the coverage $\theta(T) = A(T)/A_{max}$ and, consequently, the fraction of empty surface sites $[1 - \theta(T)]$. The equilibrium constant (K_{ads}) of the adsorption process at any given temperature can be so described, under the Langmuir approximation, as: $K_{ads} = \theta(T)/\{[(1 - \theta(T)]P_{CO}\}$. Applying the van't Hoff equation, the angular dependence of the ln(K_{ads}) versus $1/T$ gives the adsorption energy [22,30,55,62–64].

Fig. 2 shows the dependence of ln(K_{ads}) versus $1/T$ for the carbonylic species observed on the sintered MgO sample (open symbols). We observe a good linear correlation in all cases, which makes confident about the validity of the adopted model. The slopes of the lines of Fig. 2 give the adsorption enthalpies, which result similar for CO adsorbed on edge positions: 21.9 and 22.6 kJ/mol (as evaluated from the 2161 and 2170 cm^{-1} bands, respectively). As for the band due to CO adsorbed on regular (1 0 0) terraces, the measured adsorption enthalpy is much lower, i.e. 12.5 kJ/mol only. Unfortunately, the intensity of the 2203 cm^{-1} band, due to Mg_{3c}^{2+}(CO) complexes formed on corners, is not changing substantially in the 60–300 K interval upon P_{CO}, because the corresponding sites are almost fully saturated even at RT and higher temperatures are required to modify the coverage. The authors were so unable to extract from their data the ΔH_{ads} for the Mg_{3c}^{2+}(CO) complexes. The evaluation of the CO adsorption enthalpies in the case of hsa MgO sample was not possible, because the spectra are too much complex to allow a precise estimation of the integrated area for each species. Summarizing, FT-IR spectroscopy at variable T allowed to estimate separately the ΔH_{ads} values of individual species. It is worth mentioning that this result differentiates this technique from microcalorimetry, which always gives average values for all species.

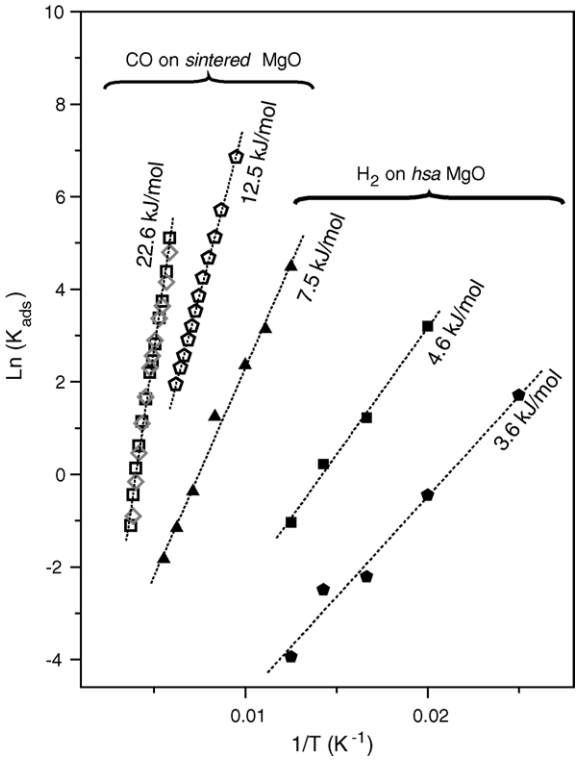

Fig. 2. Dependence of ln(K_{ads}) as a function of ($1/T$) for linear CO (open symbols) and H_2 (full symbols) molecularly adsorbed at the surface of sintered and hsa MgO on different cationic sites: Mg_{3c}^{2+} (triangles), Mg_{4c}^{2+} (squares) and Mg_{5c}^{2+} (pentagons). In the case of CO, the results of adsorption of bridged CO on Mg_{4c}^{2+} are also reported (open diamonds). The adsorption enthalpies obtained for each sites are reported in kJ/mol. Adapted from Ref. [22], with permission. Copyright (2004) by Elsevier, and from Ref. [79], with permission. Copyright (2004) by ACS.

3.1.2. CO oligomerization on low coordinated O^{2-} sites

In addition to the species formed by interaction of CO with the positive Mg^{2+} surface centers, the properties of the CO/MgO system are also characterized by the presence of negative species formed on low coordinated basic O^{2-} centers. Pioneering studies in this direction have been performed on samples activated at moderate temperatures and still covered by a fair number of OH groups [52]. Under these conditions CO was adsorbed as carbonate-like species only in presence of O_2. Successive studies performed on totally dehydrated samples and in absence of O_2, have shown that CO chemisorption leads to formation of colored anionic polymeric species [5,23–26,52–57,62,65,66]. Experimental data on powdered MgO samples demonstrated that a great number of species are formed upon interaction with carbon monoxide at 300 K, through a complex sequence of surface reactions involving the most basic surface O^{2-} ions. Some of these reactions are activated and, at RT, they need considerable time to be completed, with formation of oligomeric pink colored species [5,9,22,24,25,52,53,56,66–68]. The detailed description of these processes is of high

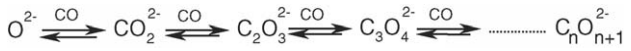

Scheme 1.

interest, because it represents one of the best examples of how highly basic oxygen species present at defect sites can attack the relatively unreactive CO molecule. In other words they can represent good examples for inspiring the design of new CO activation routes.

It is generally accepted that all the olygomeric species are originated from a common CO_2^{2-} precursor generated from a primary attack of carbon monoxide on the low coordinated O_{3c}^{2-} and O_{4c}^{2-} oxygen ions present at defect sites like corners, edges, kinks, etc. [9,22]. At low temperature ($T \approx 100$ K), the hypothesized reaction sequence is that reported in Scheme 1, leading to the formation of a complex and time dependent population of charged monomers, dimers, trimers, and oligomers. Only at RT disproportionation products (carbonates, squarate or rhodizonate anions) are slowly formed, according to the reaction depicted in Scheme 2.

It is thus clear that, in order to follow the oligomerization reaction in ''clean'' conditions (i.e. without disproportionation products) it is necessary to perform low temperature experiments. It can be noticed that the species formed in the reactions previously discussed incorporate the pristine highly basic O_{3c}^{2-} and O_{4c}^{2-} centers into more complex structures where the negative charge is delocalized on a larger set of carbon and oxygen atoms. The stability of these structures on the surface will consequently depend very much on the Coulombic interactions with the surface ions and more specifically on the distribution of the positive centers interacting with the negative parts of the admolecule. Therefore, it is expected that the structure of these species and the structure of the adsorbing centers should be closely complementary and connected via a surface-molecule recognition relation. On this basis, it is evident that the detailed knowledge of the structure of the species formed at lowest temperatures (where surface rearrangements and migrations are suppressed) gives indirect information on the structure of the adsorbing centers.

With the aim of elucidating the energetic and spectroscopic characteristics of the olygomerization reactions some of us [22] have very recently coupled a simple theoretical study (at the B3-LYP level) with an extensive experimental investigation based on time/pressure dependent IR study of CO adsorption on hsa MgO at 60 K. The choice of the temperature has been dictated by the need to minimize surface rearrangement upon interaction with CO and to suppress the disproportionation reactions, without causing CO liquefaction.

The IR spectra in the 2120–2050 and 1700–1125 cm^{-1} intervals of CO adsorbed at 60 K on a high surface area MgO

Scheme 2.

sample are shown as a function of the CO coverage in Fig. 3, which refers to the chemistry of CO interacting with low coordinated O^{2-} basic centers and thus represents the low frequency counterpart of Fig. 1a, which refers to the chemistry of Mg^{2+}(CO) adducts. These spectra represent the first IR investigation of the interaction of CO with polycrystalline MgO powders below the liquid nitrogen temperature and differ from those obtained in the past at higher T (about 100 K) [9,24]. The differences are mainly due to the fact that at 60 K higher CO coverages can be obtained as compared to those obtained for similar P_{CO} in experiments performed around 100 K. The most intense spectrum in Fig. 3 corresponds to $P_{CO} = 40$ Torr; the other spectra were obtained by decreasing the pressure in steps at $T = 60$ K. The spectrum with lowest intensity has been obtained after prolonged pumping at 60 K and corresponds to P_{CO} lower than 10^{-3} Torr. The original spectrum at higher pressure can be restored by redosing CO at 60 K, so indicating that the responsible species are completely reversible and involve surface processes characterized by very low or negligible activation barriers with respect to kT.

The spectra reported in Fig. 3 can be discussed, coming from the lowest to the highest P_{CO}, in terms of (i) formation of carbonate CO_2^{2-} and dimeric $(C_2O_3)^{2-}$ species on the less reactive O^{2-} sites and (ii) formation of trimeric $(C_3O_4)^{2-}$ species on more reactive O^{2-} sites and their evolution into oligomeric species. Starting with the first point (i), the peaks at 1316 cm^{-1} (very sharp and intense) and at 1279 cm^{-1} (broader and weaker), which are two of the most important IR manifestations observed at lowest CO coverages (see A doublet in Fig. 3), have been ascribed to the asymmetric and symmetric stretching modes of the CO_2^{2-} structure [22]. The assignment of this doublet, already observed in previous experiments performed at higher temperatures [5,9,24], is in agreement with ab initio calculations [22], which predict a correct baricenter of the IR modes. The nearly immediate formation of these species at a temperature as low as 60 K indicates that the involved reaction (first equilibrium in the reaction reported in Scheme 1) is substantially not activated. This experimental evidence well agrees with the high stability of the calculated adducts (218 kJ/mol) [22]. The 1316–1279 cm^{-1} doublet of carbonate CO_2^{2-} species A saturate after the first three spectra reported in Fig. 3 and then progressively disappears; at the same time a new triplet grows at 1635 cm^{-1} (M), 1476 cm^{-1} (S) and 1344 cm^{-1} (W) (bands labeled as D species in Fig. 3). According with ab initio calculation, the triplet is considered the consequence of further CO addition on the pre-formed A species, finally resulting in the formation of $(C_2O_3)^{2-}$ species. In the P_{CO} range covered by Spoto's experiments [22] no further CO addition involving this surface sites has been observed, testifying that the energy barrier associated with the formation of a trimeric species $(C_3O_4)^{2-}$ is much higher than kT at 60 K for the sites giving rise to the A and then to D species. Conversely, the activation barrier for the formation of dimeric species $(C_2O_3)^{2-}$ is in the range of kT as it has been overcame by a P_{CO} increase.

Coming to the second point (ii), together with the A doublet, the low P_{CO} spectra reported in Fig. 3 are dominated by two set of five bands (labeled as C and C′). According to results

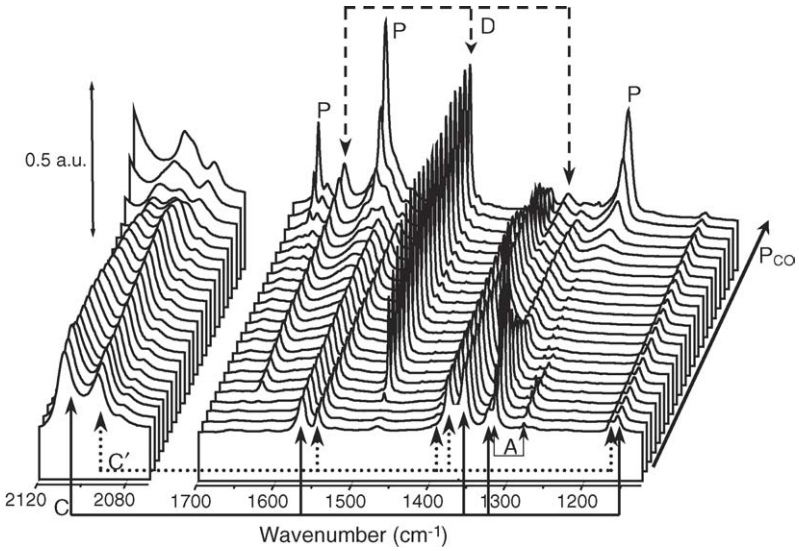

Fig. 3. Coverage dependence of the IR spectra of CO dosed at 60 K on a hsa (230 $m^2\ g^{-1}$) MgO sample, increasing CO coverages from front to back spectra. The reported spectroscopic regions (2120–2070 and 1700–1125 cm^{-1}) refer to the chemistry of CO interacting with low coordinated O^{2-} basic centers. Labels A, D, C (C′) and P refer to bands ascribed to CO_2^{2-} carbonites, $(C_2O_3)^{2-}$ dimers, $(C_3O_4)^{2-}$ trimers and polymeric $(C_nO_{n+1})^{2-}$ species, respectively. Adapted from Ref. [22], with permission. Copyright (2004) by Elsevier.

emerging from the ab initio study reported in Ref. [22], each group of five bands has been ascribed to the five (ν_1, ν_2, ν_3, ν_{3a} and ν_4) modes of trimeric $(C_3O_4)^{2-}$ species hosted on two slightly different surface sites (see Table 1). It is worth noticing that the band $\tilde{\nu}_{3a}$ was not assigned in older works [5,24,69,70]. According to the relative intensities of the five components of the two sets of five bands, the relative abundance of C and C′ species has been estimated to be ≈60 and ≈40%, respectively. A third component appears in the two modes characterized by the stronger IR bands (ν_1 and ν_3). These additional IR features have been assigned to a third family (C″) of $(C_3O_4)^{2-}$ species with a very low surface abundance (less than 5%) to allow the detection of the more IR active modes only (see Table 1).

As the trimeric $(C_3O_4)^{2-}$ species C, C′ and C″ have been observed at 60 K even at the lowest P_{CO} values, the adsorption of up to three CO molecules on those surface sites must be an almost non-activated process. When P_{CO} is further increased, the bands of the trimeric species (C, C′ and C″) decrease simultaneously without disappearing completely, see Fig. 3, while several new bands grow up. Among them the most intense are observed at 1668 cm^{-1} (S), 1580 cm^{-1} (VS) and 1266 cm^{-1} (VS) (bands "P" in Fig. 3). This process is reversible, since a successive decrement of the P_{CO} restores the initial situation, and this implies that both the enthalpy and the activation energy for the formation of polymeric species on those surface sites are modest. The calculated instability of the tetramer [22] suggests that the new bands observed are due to pentamers or to oligomers of higher nuclearity.

3.1.3. Conclusive remarks: the novelties arising from experiments of CO adsorbed at 60 K

The experiments discussed in the previous sections represent the first FT-IR investigation of the interaction of CO with polycrystalline MgO powders below the liquid nitrogen temperature. The adoption of low temperature conditions has been proved to be necessary in order to avoid the formation of disproportionation products during the CO olygomerization reaction occurring on the low coordinated O^{2-} sites. Only in these conditions, the detailed knowledge of the structure of the formed olygomeric species can give indirect information on the structure of the adsorbing centers. It is worth underlining that, if T is increased from 60 up to 100 K, at constant P_{CO}, the IR spectrum of adsorbed species changes dramatically and becomes similar to that observed and discussed in previous

Table 1
IR frequencies of the five modes (ν_1, ν_2, ν_3, ν_{3a} and ν_4) of the trimeric $(C_3O_4)^{2-}$ species formed at 60 K on three different basic surface sites (species labeled as C, C′ and C″) of high surface area MgO, compared with those obtained with ab initio calculations, from Ref. [22]

IR mode	Site C (cm^{-1})	Site C′ (cm^{-1})	Site C″ (cm^{-1})	I_{exp} (a.u.)	ab initio model (cm^{-1})	I_{theo} (a.u.)
ν_1	2108	2093	2084	S	2122	S
ν_2	1566	1543	n.o.	M	1492	M
ν_3	1355	1376	1398	S	1368	S
ν_{3a}	1324	1318	n.o.	M	1306	M
ν_4	1157	1166	n.o.	W	1161	W

The relative surface abundance of C, C′ and C″ species is: ∼60, ∼40 and less than 5%, respectively. Also the relative intensity of the five modes in both experimental (I_{exp}) and theoretical (I_{theo}) spectra are reported. For the less populated C″ site, only the most intense IR modes have been observed. n.o.: not observed; S: strong; M: medium; W: weak.

contributions [9,24,52,53,67]. The species formed at higher temperature (100 K) are irreversible and cannot be removed by pumping. This means that the formation of polymeric species at 100 K is associated to higher activation energies. Spoto et al. [22] hypothesized that the increment of the energy barrier is due to an activated surface rearrangement.

In conclusion, the investigation of CO olygomerization on hsa MgO conducted at 60 K gave the opportunity of studying monomeric and oligomeric precursors of the polymeric species described in Refs. [9,24,53], stable at higher temperatures. As these species are formed without substantial activation barrier, they directly reflect the topology of the MgO surface. These recent results well illustrate the extreme complexity of the processes occurring at the surface of hsa MgO when a large temperature interval is considered, adding new information on the interaction of CO probe with surface cations and anions, so that a much more complete view on the topic has been reached. In other words, the experiments here reviewed well show the utility of the low temperature experiments in improving the knowledge of the structure of the surface sites with respect to the experiments performed at higher temperature. Finally, a further contribution to the understanding of the surface properties comes from the study of the temperature dependance of the intensity of the IR features of CO adsorbed on individual Mg^{2+} adsorption sites, which allows the determination of site-specific adsorption enthalpies.

3.2. H_2 adsorption on high surface area MgO surface: FT-IR experiments at 20 K

The study of H_2 adsorption on oxides is of relevant importance within the framework of the vast theme of hydrogen activation on solid surfaces, finding application in catalysis [9] and hydrogen storage [71]. As far as catalysis is concerned, hydrogenation, dehydrogenation and hydrogen transfer reactions are known to occur at the surface of α-Cr_2O_3 and other oxides containing transition metal ions with partially filled d-shell [9]. Systems incorporating metal ions in d^{10} or d^0 electronic configuration (either metal oxides like ZnO or MgO or oxidic materials like exchanged zeolites) are generally less active but nevertheless important, at least for fundamental studies, because of their ability to dissociate the hydrogen molecule. The investigation of the surface properties of oxides toward the H–H bond activation is also of importance because of the analogies with the C–H bond activation, a topic occupying a central position in industrial processes. In this respect, it has been for instance shown that the sites responsible for H_2 dissociation on MgO are also active in the C–H cleavage [72].

3.2.1. H_2 splitting investigated at RT

Before facing the spectroscopy of H_2 adsorption on MgO samples at low temperature, some general comments on the spectra obtained upon dosing at room temperature dihydrogen on hsa MgO are due. The H_2 adsorption on MgO can in principle be either molecular or dissociative. Dissociative adsorption of hydrogen on hsa MgO has been already reported and two different paths have been proposed: *homolytic* and *heterolytic* [9]. Homolytic splitting operates under UV-irradiation only [73–75] and will not be further discussed here. Heterolytic splitting takes place at 300 K, without the help of ultraviolet photons, on coordinatively unsaturated (cus) $Mg^{2+}O^{2-}$ surface pairs, following the surface reaction depicted in Scheme 3.

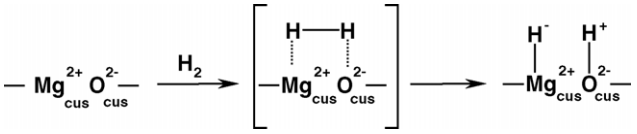

Scheme 3.

From literature data, it emerges that two different families of hydrides (Mg–H) and hydroxyls (O^{2-}–H) groups are formed at RT, differing for their vibrational properties and their behavior upon P_{H_2} changes. The first family (hereafter family I) is characterized by two intense and narrow IR peaks at 1325 and 3462 cm^{-1} (see Fig. 4), corresponding to the ν(MgH) and ν(OH) modes, respectively. These species are reversible at RT upon reducing P_{H_2}, suggesting that the two fragments are either in adjacent position or, if adsorbed at distant positions, able to easily migrate on the surface to recombine and give back molecular hydrogen [57,76,77]. Knözinger et al. hypothesized that the splitting process occurs on highly unsaturated surface sites [57]. Opposite to the family I of hydride and hydroxyls groups, the second one (hereafter family II) is more stable and is characterized by a ν(MgH) mode at 1125 cm^{-1} (broad band) and by a ν(OH) mode at 3712 cm^{-1} (sharp band), see Fig. 4. The intensity of these bands is highly dependent upon the MgO surface area and the outgassing temperature [57]. Family II has been recently assigned to the result of a heterolytic splitting process occurring at inverse corner sites [78,79]. Note that a third family of hydride and hydroxyl species (family III in Fig. 4) has been recently discovered [79] upon lowering the temperature from RT to 20 K, as it will be discussed in Section 3.2.4.

3.2.2. The identification of the molecularly adsorbed intermediate species

RT experiments have not been able to detect the molecularly adsorbed intermediate species, implying that the activation barrier associated with the H_2 dissociation reaction is negligible at RT, so that the splitting reaction is very fast. The possibility to detect molecularly adsorbed H_2 molecules lies, therefore, in the ability to strongly reduce *T*, as demonstrated by the recent work of Gribov et al. [79]. Before discussing the observation of the intermediate species, let us resume the main features characterizing the spectra of H_2 adsorbed at 20 K on hsa MgO. Fig. 5 shows the IR spectra of H_2 adsorbed at 20 K on a hsa (230 $m^2\ g^{-1}$) MgO sample as a function of H_2 coverage θ. To discriminate between contact time and P_{H_2} effects, Gribov et al. [79] adopted the following experimental strategy. A P_{H_2} of 10 mbar has been initially dosed at 20 K on the sample and an elapsed time of up to 1 h was adopted. Once the IR spectra do not show any further evolution with time, then the authors

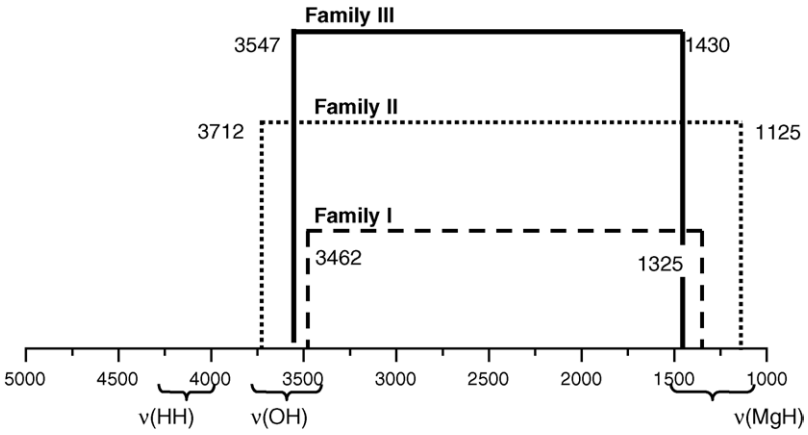

Fig. 4. Schematic representation of hydride and hydroxyls stretching modes observed upon dosing H_2 on hsa MgO sample. Families I and II are directly observed in RT experiments, while family III has been observed only upon cooling the MgO/H_2 system below 180 K, as discussed successively in Section 3.2.2. Unpublished figure.

started to progressively reduce P_{H_2} down to less than 10^{-3} mbar (from back to front in Fig. 5). Focusing the attention on the hydroxyls and hydrides regions, the same families (I and II) of hydrides and hydroxyls groups discussed in the case of adsorption at RT are formed even when H_2 is dosed on MgO samples pre-cooled at 20 K, indicating that the involved sites are very active toward H_2 dissociation [79]. Upon increasing the H_2 equilibrium pressures, the peaks related with family I species become broader and move simultaneously upward (from 3454 to 3460 cm^{-1}) and downward (from 1325 to 1306 cm^{-1}), while the peaks related to family II species show a little tendency to shift. Both families I and II are irreversible at 20 K.

Together with the products of H_2 splitting, at high H_2 coverage, Gribov et al. [79] detected, for the first time, complex and intense absorptions in the 4800–4000 cm^{-1} interval. As this is the spectral region where the ν(HH) mode of molecularly adsorbed H_2 is expected [30,63,80–90], the authors ascribed the three complex components centered at about 4126–4122, 4099–4093 and 4081–4076 cm^{-1} to $Mg_{5c}^{2+}(H_2)$, $Mg_{4c}^{2+}(H_2)$ and $Mg_{3c}^{2+}(H_2)$ molecular adducts, respectively. The expected *ortho–para* splitting (of 6 cm^{-1}) is clearly visible for the doublet at 4099–4093 cm^{-1}, while just results in a band broadening for the remaining two. These values are significantly downward shifted with respect to the ν(HH) mode of the unperturbed H_2 molecule measured in the gas phase by Raman spectroscopy: $\tilde{\nu}(HH) = 4161$ and 4155 cm^{-1} for the *ortho* and *para* H_2, respectively. The assignment of Gribov et al. [79] reflects thus the increased weakening of the H–H bond strength expected by moving from the adduct formed on a five-coordinated, Mg_{5c}^{2+} magnesium cation (regular (1 0 0) surface site), through the complex formed on a four-coordinated Mg_{4c}^{2+} cation (step site), to the adduct formed on a three coordinated Mg_{3c}^{2+} cation (corner site): $\Delta\tilde{\nu}(HH) \sim -38, -62$ and -80 cm^{-1}, respectively.

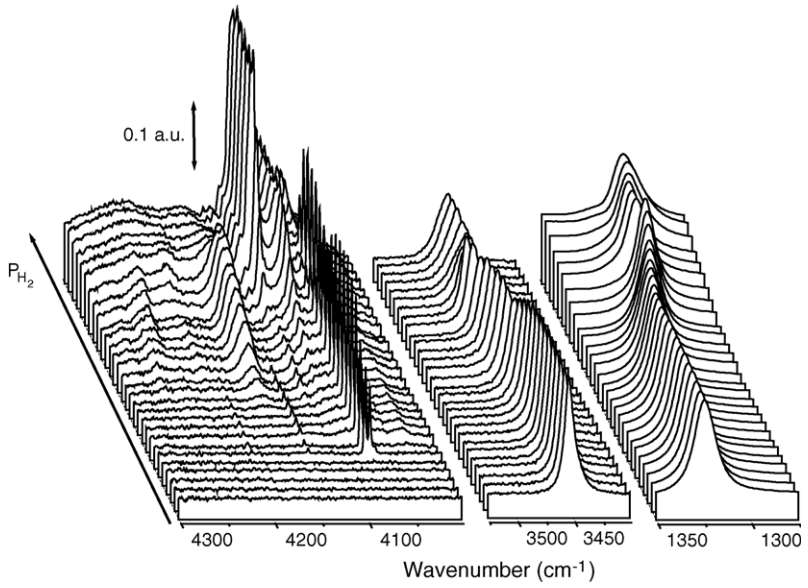

Fig. 5. Pressure dependence of the IR spectra of H_2 adsorbed at 20 K on a hsa (230 m^2 g^{-1}) MgO sample. The back spectrum has been collected after an elapsed time allowing the surface species to reach the equilibrium conditions and corresponds to the maximum H_2 coverage ($P_{H_2} = 10$ mbar), while the front spectrum has been recorded after prolonged outgassing at 20 K ($P_{H_2} < 10^{-3}$ mbar). Adapted from Ref. [79], with permission. Copyright (2004) by ACS.

It is useful to recall at this point that the experiment illustrated in Fig. 5 shows the effect of the H_2 pressure on the spectra of the molecularly and dissociatively adsorbed species after full equilibration of the H_2/MgO system at 20 K. It is however noticeable that, when hydrogen is dosed on hsa MgO pre-cooled at 20 K, a dependence of the spectrum on contact time is observed before equilibration is reached. This effect is shown in Fig. 6. Beside the three already discussed bands in the ν(HH) region a fourth one, exhibiting a much broader character, is clearly evident at 4031 cm^{-1} in the black bold spectrum of Fig. 6. Contrarily to the previously assigned bands, this component, undoubtedly associated with a new molecularly adsorbed hydrogen species characterized by an even greater activation of the H–H bond, gradually decreases with time, see thin curves in Fig. 6. After 1 h of contact at 20 K, the 4031 cm^{-1} component is totally eroded (gray bold curve in Fig. 6, corresponding to the back spectrum in Fig. 5) demonstrating the transient nature of this fourth molecular H_2 surface adduct. The progressive disappearance of the 4031 cm^{-1} band is accompanied in the ν(OH) and in the ν(MgH) stretching regions by a significant increase of two bands at 3460 and 1306 cm^{-1}. As these frequencies are very close to those already observed in the RT experiments and ascribed to family I (see Fig. 4), the experiment of Gribov et al. [79] demonstrates that the splitting of H_2 and the consequent formation of the hydrides and hydroxyls groups belonging to family I passes through the formation of a transient molecular adduct characterized by a ν(HH) of 4031 cm^{-1}. The possibility to detect this band only at 20 K and its behavior with time implies that the activation energy associated with the H_2 splitting reaction is negligible at RT, while it becomes comparable (slightly higher) than kT at 20 K. Conversely, the formation of the hydrides and hydroxyls groups belonging to family II is still immediate even at 20 K, implying an energy barrier much lower than kT even at 20 K, and thus explaining the impossibility to detect the intermediate molecular adduct under these experimental conditions.

3.2.3. Evaluation of the adsorption energy for molecular adsorbed H_2 adducts

In the previous section, we have discussed the effect that a P_{H_2} variation has on the IR spectra of the MgO/H_2 system in equilibrium conditions as far as the surface molecular bonded and heterolitically adsorbed species are concerned. In that experiment the thermodynamic parameter T was kept constant at 20 K. Gribov et al. [79], starting from the same initial conditions, have also performed experiments where the P_{H_2} was kept constant and the T was progressively increased. In such isobaric experiment they observed the progressive desorption of the most labile species which are, in the desorption order, the $Mg_{5c}^{2+}(H_2)$, $Mg_{4c}^{2+}(H_2)$ and $Mg_{3c}^{2+}(H_2)$ molecular adducts. By applying the same method previously discussed for the CO adsorption on the Mg^{2+} sites (vide supra Section 3.1.1), authors [79] obtained the specific adsorption energy for the formation of the molecular adducts: these were 3.6 kJ/mol for the $Mg_{5c}^{2+}(H_2)$ adducts on regular (1 0 0) planes; 4.6 kJ/mol for the $Mg_{4c}^{2+}(H_2)$ species on edges and 7.5 kJ/mol for the $Mg_{3c}^{2+}(H_2)$ ones on corners (see Fig. 2).

3.2.4. Conclusive remarks: the novelties arising from experiments of H_2 adsorbed at 20 K

Splitting of hydrogen at RT on $Mg^{2+}O^{2-}$ surface pairs and the consequent formation of families of hydroxyl and hydride species was already described in the literature concerning RT experiments. It is worth recalling that in such conditions it was however not possible to detect molecularly adsorbed precursors (if any) in the dissociation reaction. This goal has been achieved by Gribov et al. [79] by experiments performed at 20 K, which allowed to observe, for the first time, transient molecular precursor of the hydride and hydroxyl species belonging to

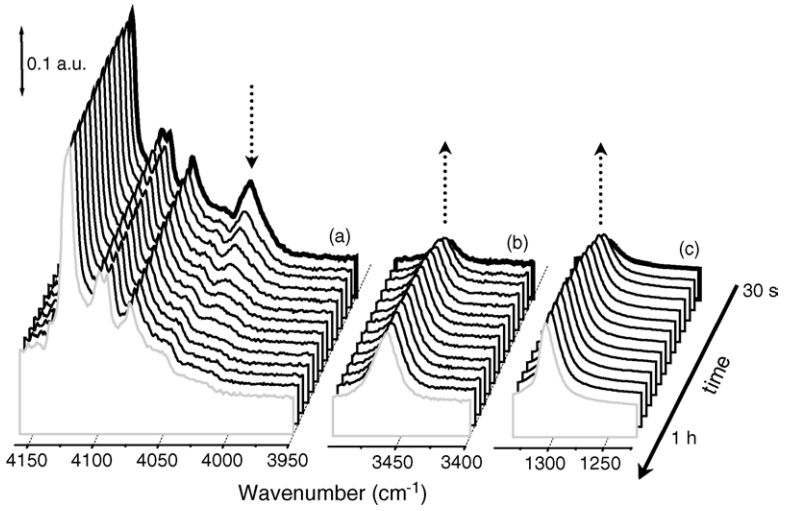

Fig. 6. Dependence on the contact time of the spectrum of H_2 adsorbed at 20 K on hsa MgO (230 $m^2\ g^{-1}$). For clarity, only the ν(HH) (4160–3950 cm^{-1}) region and the ν(OH) (3520–3380 cm^{-1}) and ν(MgH) (1360–1260 cm^{-1}) regions of family I are shown (parts a, b and c, respectively), as the ν(OH) and ν(MgH) modes of family II do not show any appreciable time dependence. Bold black line: immediately after the dosage of 10 mbar of H_2 on the sample pre-cooled at 20 K. Bold gray line: after one hour of contact at 20 K. Light black lines: intermediate contact times. The arrows show the evolution of the spectra with time. Adapted from Ref. [79], with permission. Copyright (2004) by ACS.

family I (Fig. 6). This makes possible to establish an energetic scale in the activation barrier of the heterolytic H_2 dissociation between hydroxyl and hydride species belonging to families I and II.

Furthermore, in addition to those already known, the formation of a third family of hydroxyl and hydride species was discovered to occur [79] when H_2 is first dosed at RT on a hsa MgO sample and the *T* then gradually lowered down to 20 K in H_2 atmosphere. Following this procedure, at about 180 K, a new couple of bands appears at 3547 and 1430 cm^{-1} which are assigned to the ν(MgH) and ν(OH) modes of a third family of hydroxyl and hydride species, as anticipated in Fig. 4, which are not reversible upon decreasing P_{H_2} down to 10^{-3} mbar at 20 K.

Combining all this set of time-, pressure- and temperature-dependent IR studies with parallel high resolution TEM and AFM investigations Gribov et al. [79] have been able to give an assignment of the three families of hydroxyl and hydride species, as summarized in Fig. 4, on a local structural ground. Without entering in the details of the arguments resulting in the assignment, we just report here the conclusions, by recalling that inverse anionic and cationic corners play a key role in the H_2 splitting. Family I corresponds to H^+ coordinated to three O^{2-} surface anions and to H^- coordinated to two surface Mg^{2+} cations. Family II is due to H^+ coordinated to one O^{2-} surface anions and to H^- coordinated to three surface Mg^{2+} cations. Finally, family III corresponds to H^+ coordinated to two O^{2-} surface anions and to H^- coordinated to one surface Mg^{2+} cations. In conclusion, the low temperature experiments here reviewed represent a nice example of the improvements which can be reached in the structural characterization of the oxide surface with respect to the conventional experiments carried out at RT.

3.3. H_2 adsorption on exchanged Cu^+-ZSM-5: FT-IR experiments at 20 K

The potentialities of monitoring by means of FT-IR spectroscopy the adsorption of probe molecules at temperature lower than liquid nitrogen have been recently extended also to microporous systems, such as zeolites and MOFs [30,50,51,91]. As an example, we report here the recent results obtained on a Cu^+ exchanged ZSM-5 zeolite, by following the evolution of $Cu^+(H_2)$ adducts as a function of H_2 pressure and temperature. It is well known that the extraframework Cu^+ counterions in Cu^+-ZSM-5 present very peculiar chemical properties, such as a specific catalytic activity in deNO_x reactions [92] and the ability to form uncommon complexes like the homopletic $[Cu(CO)_3]^+$ tri-carbonyl [31,32,36,38] and the $Cu^+(N_2)$ dinitrogen adducts [29,31]. This is mainly due to the structure of the Cu^+ ions, which are highly coordinatively unsaturated and thus easily accessible to molecules moving inside the zeolite channels [34,39,42]. Very recently, it has been reported that intrazeolitic Cu^+ species can also bind molecular H_2 at room temperature [30,93,94], a rather surprising finding when considering that the only $Cu^+(H_2)$ complex previously known was the [Cu(η^2-H_2)Cl] adduct isolated by co-condensation of CuCl and H_2 in an Ar matrix [95]. The interest of a microporous system able to reversibly adsorb H_2 at room temperature is self-evident, because it satisfies one of the pre-requisites for hydrogen storage [71].

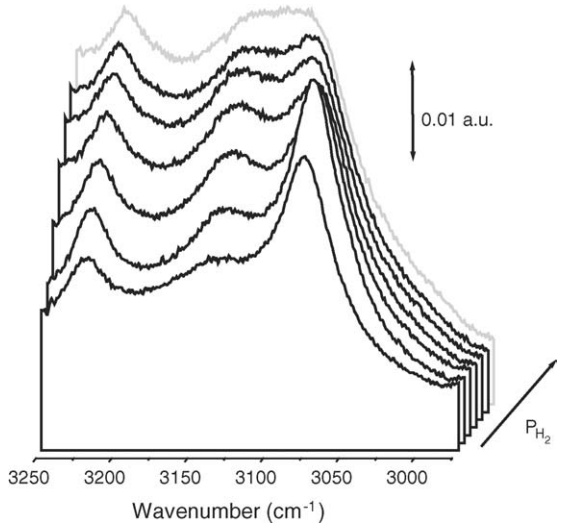

Fig. 7. IR spectra of H_2 adsorbed on Cu^+-ZSM-5 (previously outgassed for 1 h at 773 K) as a function of the gas phase equilibrium pressure (upper curve, gray: 20 Torr; lower curve: $<1 \times 10^{-3}$ Torr) at constant temperature (15 K). Adapted from Ref. [30], with permission. Copyright (2004) by RSC.

3.3.1. Evolution of the $Cu^+(H_2)$ adducts at 15 K as a function of H_2 pressure

Fig. 7 illustrates the effect of reducing the P_{H_2} at the constant temperature of 15 K on Cu^+-ZSM-5. The $Cu^+(H_2)$ interaction at P_{H_2} below 10^{-3} Torr, front spectrum in Fig. 7, gives rise to absorptions at 3222 cm^{-1} (very weak), ca. 3130 cm^{-1} (very weak and broad) and 3079 cm^{-1} (weak but well defined). According to the work of Plitt et al. [95] on the [Cu(η^2-H_2)Cl] adducts isolated in Ar matrix the highest frequency component is assigned to H_2 adsorbed on residual CuCl nanoclusters entrapped in the zeolitic channels after the ion exchange procedure and not completely removed by the activation procedure. The bands at 3130 and 3079 cm^{-1} are assigned to similar $Cu^+(H_2)$ adducts formed on the ions counterbalancing the ZSM-5 framework negative charge. The presence of a doublet can be accounted for by recalling that in the ZSM-5 structure Cu^+ can occupy slightly different locations [29,31,96] differing for the number of framework oxygen ligands entering the Cu^+ first coordination sphere. It is worth noticing that H_2 is able to distinguish between these two different types of sites, giving rise to two bands separated by 51 cm^{-1}. This is a consequence of the fact that we are perturbing a single bond H–H (vide supra Section 1.). This was not the case of probes characterized by triple bonds, like C≡O, N≡O or N≡N, that were unable to distinguish between adducts formed on the two different families of sites [29,31,32,36,38]. The component at 3130 cm^{-1}, characterized by the lower $|\Delta\tilde{\nu}(HH)|$, is ascribed to $Cu^+(H_2)$ adducts formed on three-fold coordinated cuprous ions, while that at 3079 cm^{-1} is due to $Cu^+(H_2)$ adducts adsorbed on more coordinatively unsaturated Cu^+ cations (exhibiting only two framework oxygen atoms in their coordination sphere) [30].

The downward shift ($\Delta\tilde{\nu}(HH) = -1030$ and $-1080\ cm^{-1}$) with respect to unperturbed gaseous H_2 (Raman band at $4161\ cm^{-1}$) is remarkable when compared with analogous complexes formed upon dosing H_2 on Na-ZSM-5, where $\Delta\tilde{\nu}(HH)$ is $-61\ cm^{-1}$ [30,77]. It is widespread opinion that a large shift (of the order of $-1000\ cm^{-1}$) of the $\tilde{\nu}(HH)$ frequency in $Cu^+(H_2)$ molecular complexes in side-on configuration is the symptom of a strong interaction involving weak electrostatic (charge-induced dipole and charge quadrupole) and strong chemical (donation from the H_2 σ orbital and back-donation from the 3dπ Cu^+ orbitals) contributions [30,93,95,97]. The σ donation in the 4s orbital and back-donation from the dπ orbitals of Cu^+ are synergistic and lead to the formation of three center $Cu^+(H_2)$ covalent bonds, where back-donation weakens the H–H bond to a very large extent. This is reflected in the relatively large interaction energy (60–80 kJ mol^{-1}) [30,93,95]. The covalent character of the Cu^+–H bonds in the side-on $Cu^+(H_2)$ species also accounts for the low intensity of the $\tilde{\nu}(HH)$ mode because the H–H stretching is not accompanied by strong dipole oscillations along the covalent $Cu^+(H_2)$ and H–H bonds.

The upward shift (and broadening) of both 3130 and 3079 cm^{-1} bands upon increasing P_{H_2}, see the front to back evolution in the spectra reported in Fig. 7, is due to solvatation and transformation of the pristine $Cu^+(H_2)$ into $Cu^+(H_2)_n$ polynuclear adducts occurring when the zeolite channels are filled by a H_2 liquid-like phase. This is accompanied by weakening of the $Cu^+\cdots H_2$ interaction and, consequently, by a shift of the $\tilde{\nu}(HH)$ band toward that of gas phase H_2 [30,97]. A successive prolonged outgassing at 15 K restores the spectrum previously discussed (front spectrum in Fig. 7), meaning that we are dealing with species irreversible at this temperature.

3.3.2. Evolution of the $Cu^+(H_2)$ adducts at constant H_2 pressure as a function of temperature

Fig. 8 shows the spectra obtained upon dosage of hydrogen at 300 K (front spectrum) and by progressive lowering of the temperature down to 15 K (back spectrum). The room temperature spectrum exhibits the same triplet than that collected at 15 K and low P_{H_2}, already discussed above (see front spectrum in Fig. 7). The differences in the IR features concern the lower intensity, the broader character and the reversibility upon outgassing. The effects of the temperature decrease on the IR features can be commented by dividing the sequence into two ranges: 300–100 and 100–15 K. Down to 100 K we basically observe an increase of the bands intensity with a parallel narrowing (of modest entity). In the 100–15 K interval, the effect is similar to that observed upon increasing P_{H_2} at 15 K (see Fig. 7): important band broadening accompanied by a decrease of the batochromic shift of all the components. This equivalence is due to the fact that, in both experiments, the dominating effect is the progressive filling of the zeolite pores by physisorbed H_2 molecules.

The use of low temperature in the investigation of the H_2 adsorption is not mandatory in this case owing to the extraordinary ΔH value of the $Cu^+(H_2)$ adducts, but has been necessary to observe the formation of polynuclear $Cu^+(H_2)_n$ adducts, characterized by much lower adsorption enthalpies.

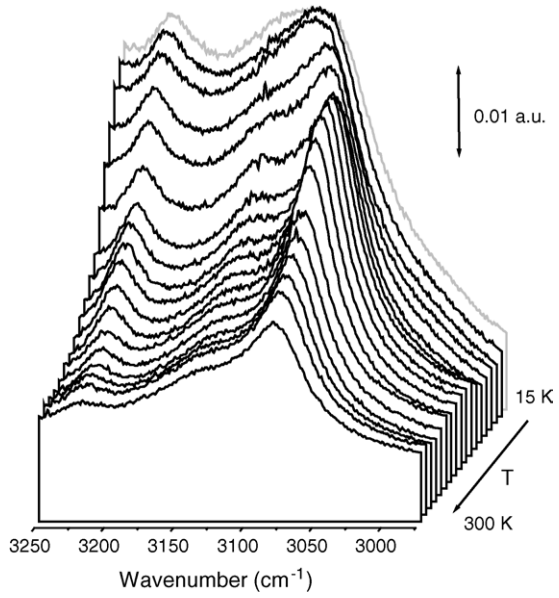

Fig. 8. IR spectra of H_2 adsorbed on Cu^+-ZSM-5 (previously outgassed for 1 h at 773 K) as a function of the temperature (varied in the 300–15 K interval) at nearly constant gas phase equilibrium pressure (20 Torr). Adapted from Ref. [30], with permission. Copyright (2004) by RSC.

3.4. Interaction of CO and H_2 with protonic sites in H-SSZ-13 zeolite

Zeolite and zeotype materials having the chabazite topology, such as H-CHA, H-SSZ-13 (the low Al zeolite with CHA structure) and H-SAPO-34, have generated a great interest in the catalytic community as H-SAPO-34 has shown to be particularly promising for the reaction where CH_3OH is converted into a mixture of light olefins and H_2O [98–101].

The chabazite lattice is composed of layers of double six-rings that are interconnected by four-rings, leading to a regular arrangement of barrel shaped cages. The cages are accessible through eight-ring windows. The chabazite structure provides four crystallographic independent oxygen atoms, labeled as O(1), O(2), O(3) and O(4) according to the nomenclature introduced by Smith et al. [102]. Consequently, the chabazite structure provides four possible acid site configurations, depending on to which oxygen atom the proton is attached: H(1), H(2), H(3) and H(4). The four site-topologies are rather similar and all protons are exposed to the cage. A minor relevant difference is that O(1), O(2) and O(4) are all parts of the eight-membered ring window, delimiting the CHA cage, while O(3) is protruding inside the cage and is not part of the open window of the cage. This characteristic, together with the fact that, in vacuum conditions, a proton in H(3) could interact with an oxygen of six-ring window, forming an H-bond, makes this site slightly different from the others and is expected to need a higher equilibrium pressures to form adducts with probe molecules.

In collaboration with the Chemistry Department of the Oslo University (Bjørgen and Lillerud), we have recently performed an IR investigation of H-SSZ-13 and of the isostructural H-SAPO-34 material, by studying CO adsorption at 70 K [50] and H_2 adsorption at 15 K [51]. The results demonstrate that H-SSZ-13 is a strong Brønsted acidic material, essentially having two distinct *families* of acidic sites. In contrast to numerous preceding reports [102,103], where only two protonic sites, H(1) and H(2) have been hypothesized to be populated, the new low temperature IR experiments highlighted a proton distributions among all four crystallographic independent sites. The new data consistently suggest that the most abundant family of protons occupies sites H(1), H(2), and H(4). Protons hosted in these three sites are almost indistinguishable on a spectroscopic ground. The second, and less abundant family, occupies site H(3). This proton is therefore only exposed to one cage.

The IR spectrum of the zeolite before molecule dosage is characterized by two families of Brønsted sites characterized by a $\tilde{\nu}$(OH) component at 3616 and 3584 cm^{-1}, see full black line curves in Fig. 9a and c, known in the literature as high frequency (HF) and low frequency (LF) component, respectively [50,51,102,103]. Note that the LF band is less intense than the HF band and, as its extinction coefficient is higher, this observation implies that the LF sites correspond to a minor fraction of the total set of proton sites in H-SSZ-13. Upon interaction with both CO and H_2 molecules (gray and dotted lines in Fig. 9a and c, respectively) the HF component is eroded first and the LF later. The same occurs when H_2O or CH_3OH are used as probes [104]. On the basis of these spectroscopic evidences Bordiga et al. [50,51,104] concluded that the HF band is due to spectroscopically indistinguishable protons H(1), H(2), and H(4), while the LF band is due to less accessible protons in the less occupied H(3) site, the only one not directly exposed to the eight-ring window.

We will now move to discuss the frequency region of the C–O stretching. The formation of hydrogen bonded adducts between strong Brønsted sites and CO molecules, is also accompanied by a perturbation of the internal vibration of the base (Fig. 9b). Starting from the lowest CO coverage, a component is clearly visible at 2177 cm^{-1}, $\Delta\tilde{\nu}(CO) = +38\,cm^{-1}$. The component is ascribed to CO adsorbed on strong bridging Brønsted acidic sites H(1), H(2), and H(4). By increasing the CO coverage we observe a gradual shift of the maximum towards lower frequency (2174 cm^{-1}) as an indication of the gradual cage filling [88] with formation also of multi adducts and of OH···CO adducts on sites H(3). Notwithstanding the frequency shift, the CO molecule has not been able to distinguish between adducts formed on HF and on LF Brønsted sites owing to the absence of two distinct C–O stretching bands. At higher P_{CO}, a component at 2164 cm^{-1} is clearly visible in Fig. 9b, and is due to the interaction between CO and external silanol groups. Coming back to the O–H stretching region (Fig. 9a) the formation of the C–O stretching band in the 2177–2174 cm^{-1} interval results in the erosion of both HF and LF Brønsted bands and to the appearance of a red-shifted band at 3300 cm^{-1},

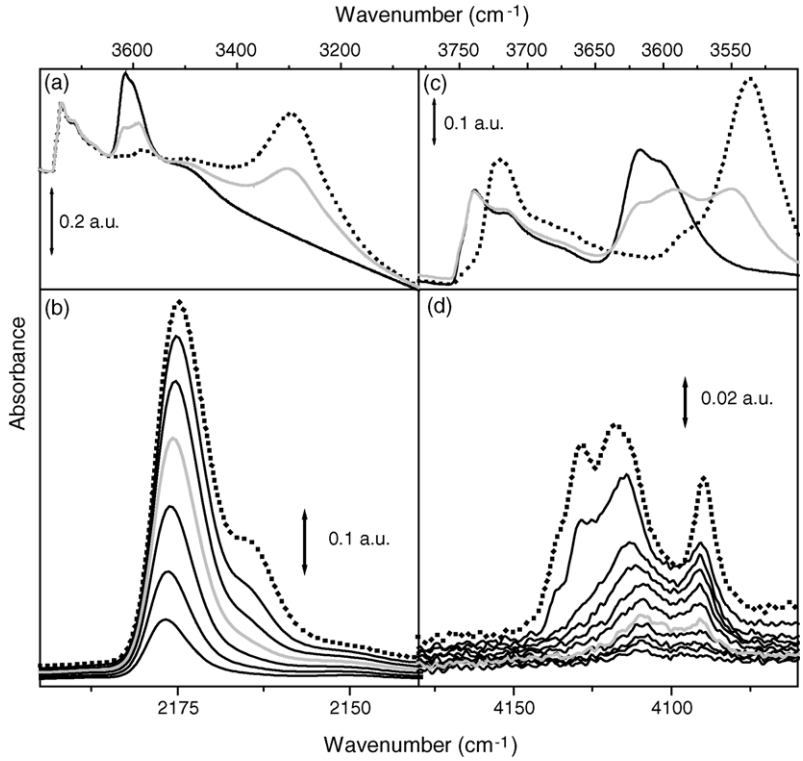

Fig. 9. IR spectra of CO and H_2 dosed on H-SSZ-13 zeolite. Parts (a) and (b) report the effect of CO dosage at 70 K in the O–H and C–O stretching regions, respectively. Part (a) shows the background, colleted before CO dosage (black full line), and two spectra recorded at increasing CO doses: gray and dotted curves, respectively. Part (b) shows background subtracted spectra collected at increasing CO coverage (gray and dotted curves refers to the spectra reported in part a). Parts (c) and (d), as parts (a) and (b) for H_2 dosed at 15 K.

$\Delta\tilde{\nu}(OH) = -316\,cm^{-1}$, due to the ν(OH) modes of OH···CO adducts. The presence of an unresolved single red-shifted ν(OH) component suggests that the acidity of the HF and LF families of Brønsted sites, measured by CO, is equivalent. This means that the HF and LF families are different under vacuum conditions (owing to a different neighbour environment), but the resulting OH···CO complexes cannot be differentiated by IR spectroscopy.

Fig. 9d reports the H–H stretching frequency region. The formation of adducts between H_2 molecules and strong Brønsted sites, testified by the consumption of the HF band (Fig. 9c), leads to the IR activation of the ν(HH) vibration of the molecule. Two bands with maxima at $4109\,cm^{-1}$, $\Delta\tilde{\nu}(HH) = -52\,cm^{-1}$, and at $4090\,cm^{-1}$, $\Delta\tilde{\nu}(HH) = -71\,cm^{-1}$, can be seen in the low coverage spectra of Fig. 9d. These shifts are comparable to those observed for H_2 interacting with defective Mg_{4c}^{2+} or Mg_{3c}^{2+} cations located at step ($\Delta\tilde{\nu}(HH) = -62\,cm^{-1}$) and corner ($\Delta\tilde{\nu}(HH) = -80\,cm^{-1}$) sites of hsa MgO, see Section 3.2.2 and Fig. 5. The component at $4109\,cm^{-1}$, growing in intensity in a parallel manner as the $3548\,cm^{-1}$ band ($\Delta\tilde{\nu}(OH) = -64\,cm^{-1}$, Fig. 9c), is inherently linked to the adduct formation between H_2 and protons located in H(1), H(2), and H(4) sites. The component at $4090\,cm^{-1}$ is less intense, even though it has an higher extinction coefficient, and should originate from the interaction of H_2 with the significantly less abundant family of sites H(3). The growth of the $4090\,cm^{-1}$ band is accompanied, in the O–H stretching region, by the complete erosion of the LF component, and by the shift of the band of engaged Brønsted sites from 3547 shifts $3536\,cm^{-1}$ (evolution from gray to dotted curve in Fig. 9c). The shift towards lower frequency of the ν(OH) component is the result of two phenomena. On one side, there is the contribution of LF species interacting very strongly with H_2, and on the other side there is the condensation of H_2 inside the pores which causes a progressive shift to lower frequencies of the overall spectrum. In the meantime, in the H–H stretching region (Fig. 9d), a new band associated with slightly perturbed H_2, appears at $4130\,cm^{-1}$ ($\Delta\tilde{\nu}(OH) = -31\,cm^{-1}$). According to the consumption of the $3740\,cm^{-1}$ band of external silanols (dotted curve in Fig. 9c), the $4130\,cm^{-1}$ band is assigned to Si–OH···H_2 adducts formed at the surface of the zeolite crystals. A parallel experiment with the isostructural H-SAPO-34 (not reported here for brevity), has shown very similar results confirming the present assignment [91].

As was the case for the Cu^+-ZSM-5 system, also in the case of the H-SSZ-13 zeolite, H_2 has shown to be a more informative probe than CO as it has been able to better discriminate between two slightly different families of adsorbing sites: two-fold versus three-fold coordinated Cu^+ ions in Cu^+-ZSM-5 and H(1), H(2), and H(4) versus H(3) sites in H-SSZ-13. This is mainly due to the fact that the same adsorbing sites are able to greatly perturb a single bond like the H–H one, rather than a triple bond like in the C≡O case, thus resulting in higher frequency shifts.

As discussed in Section 3.1.1 for the adsorption of CO on MgO and in Section 3.2.2 for the adsorption of H_2 on MgO (vide supra Fig. 2), we have quantified the adsorption energy of H_2 on the Brønsted acidic sites of the H-SSZ-13 zeolite by isobaric IR experiments in the 300–15 K temperature range. In the present case, an adsorption energy of 9.7 ± 0.3 kJ/mol was calculated, which represents a remarkable value, greater than that observed for H_2 adsorbed on the defective three-fold coordinates sites of high surface area MgO (7.5 kJ/mol, see Section 3.2.3 and Fig. 2). Clearly, H-SSZ-13 zeolite represents a rather promising example of a material where an appreciable interaction energy between hydrogen and specific surface sites is associated with a relevant storage property [51].

4. Conclusions

In this contribution we discuss recent results obtained in the field of transmission IR spectroscopy of adsorbed probe molecules by performing experiments below the liquid nitrogen temperature. The lower temperature value at which IR experiments on high surface area powdered materials were performed was limited up to now to 77 K, mainly for practical problems. This temperature frontier has been broken down very recently, thanks to the realization in our laboratory of an unique experimental set-up able to perform FT-IR experiments in transmission mode down to 15 K, on materials activated in situ under vacuum conditions ($P < 10^{-4}$ Torr) and at temperatures up to 1100 K. The lowering of the temperature below the 77 K barrier allows to use as probe molecules also those weakly interacting with the surface sites, i.e. the less perturbing ones, such as H_2 and N_2. In particular, the possibility to use H_2 opens new prospects in the discrimination among rather similar surface sites.

By illustrating as case studies the adsorption of CO and H_2 on MgO surface and the H_2 adsorption on Cu^+-ZSM-5 zeolite, we demonstrate that the experiments carried out in the 15–300 K temperature interval can be of extreme utility for complementing the experimental information on the surface structure obtained with similar experiments performed at liquid nitrogen temperature. It is demonstrated that very low temperature allows a much better comparison between results in surface science and in catalysis, mainly because of the high resolution attained at low temperature, but also because of the similarity of the observation conditions. Furthermore, it is shown that, unlike classical calorimetric experiments, where just integrated (on all adsorption sites) values are accessed, new site-specific thermodynamic data can be obtained.

Finally, the possibility to perform IR experiments in the 15–77 K range allowed us to use in an extensive way H_2 as probe molecules for surface sites. This is a great advantage as H_2 has shown a higher ability in discriminating slightly different surface sites than the more conventionally used CO or NO probes. The reason of this is mainly due to the fact that the same adsorbing sites are able to greatly perturb a single bond like the H–H one, rather than a triple bond like in the C≡O or N≡O cases, thus resulting in higher frequency shifts.

Note added in proofs

Between the manuscript submission and the proofs correction stages two important papers have been published that should not be overlooked [105,106].

Acknowledgements

We are strongly indebted with Prof. K. P. Lillerud and with Dr. M. Bjørgen (Chemistry Department of the Oslo University) for the synthesis of the H-SSZ-13 zeolite and for the friendly and scientifically stimulating interaction that we had the honor and the pleasure to have with them in the last 3 years. We acknowledge the MIUR for financial support through the NIS Centre of Excellence and INSTM through the PRISMA03 project. Laura Regli acknowledges Regione Piemonte for her Ph.D. grant.

References

[1] H. Knözinger, P. Ratnasamy, Catal. Rev.-Sci. Eng. 17 (1978) 31.
[2] A. Zecchina, E. Garrone, E. Guglilminotti, in: G.C. Bond, G. Webb (Eds.), Catalysis, vol. 6, The Royal Society of Chemistry, London, 1983
[3] A. Zecchina, C. Otero Areán, Catal. Rev.-Sci. Eng. 35 (1993) 261.
[4] J.C. Lavalley, Catal. Today 27 (1996) 377.
[5] A. Zecchina, D. Scarano, S. Bordiga, G. Ricchiardi, G. Spoto, F. Geobaldo, Catal. Today 27 (1996) 403.
[6] H. Knözinger, in: G. Ertl, H. Knözinger, J. Weitkamp (Eds.), Handbook of Heterogeneous Catalysis, vol. 2, Wiley–VCH, Weinheim, 1997, p. 707.
[7] A. Zecchina, D. Scarano, S. Bordiga, in: G. Ertl, H. Knözinger, J. Weitkamp (Eds.), Handbook of Heterogeneous Catalysis, vol. 2, Wiley–VCH, Weinheim, 1997, p. 728.
[8] A. Zecchina, C. Lamberti, S. Bordiga, Catal. Today 41 (1998) 169.
[9] A. Zecchina, D. Scarano, S. Bordiga, G. Spoto, C. Lamberti, Adv. Catal. 46 (2001) 265.
[10] C. Lamberti, E. Groppo, G. Spoto, S. Bordiga, A. Zecchina, Adv. Catal. (2006) (invited article).
[11] A. Antolini, P.J. Bradley, C. Cacciatore, D. Campi, G. Gastaldi, F. Genova, M. Iori, C. Lamberti, C. Papuzza, C. Rigo, J. Electron. Mater. 21 (1992) 233.
[12] C. Lamberti, Comput. Phys. Commun. 93 (1996) 82.
[13] C. Lamberti, S. Bordiga, F. Boscherini, S. Mobilio, S. Pascarelli, G. Gastaldi, M. Madella, C. Papuzza, C. Rigo, D. Soldani, C. Ferrari, L. Lazzarini, G. Salviati, J. Appl. Phys. 83 (1998) 1058.
[14] Y.A. Zhang, J.A. Strozier, A. Ignatiev, Phys. Rev. B 53 (1996) 7426.
[15] C. Lamberti, A. Antolini, S. Bianchi, A. Castelli, M. Dellagiovanna, Z. Phys. B: Condens. Mater. 100 (1996) 195.
[16] X.P. Xu, S.M. Vesecky, D.W. Goodman, Science 258 (1992) 788.
[17] S.C. Street, C. Xu, D.W. Goodman, Annu. Rev. Phys. Chem. 48 (1997) 43.
[18] D.C. Meier, D.W. Goodman, J. Am. Chem. Soc. 126 (2004) 1892.
[19] D. Peterka, C. Tegenkamp, K.M. Schroder, W. Ernst, H. Pfnur, Surf. Sci. 431 (1999) 146.
[20] A. Freitag, V. Staemmler, D. Cappus, C.A. Ventrice, K.A. Shamery, H. Kuhlenbeck, H.J. Freund, Chem. Phys. Lett. 210 (1993) 10.
[21] C. Xu, M. Hassel, H. Kuhlenbeck, H.J. Freund, Surf. Sci. 258 (1991) 23.
[22] G. Spoto, E.N. Gribov, G. Ricchiardi, A. Damin, D. Scarano, S. Bordiga, C. Lamberti, A. Zecchina, Prog. Surf. Sci. 76 (2004) 71.
[23] E. Escalona Platero, D. Scarano, G. Spoto, A. Zecchina, Faraday Discuss., Chem. Soc. 80 (1985) 183.
[24] A. Zecchina, S. Coluccia, G. Spoto, D. Scarano, L. Marchese, J. Chem. Soc., Faraday Trans. 86 (1990) 703.
[25] L. Marchese, S. Coluccia, G. Martra, A. Zecchina, Surf. Sci. 269/270 (1992) 135.
[26] G. Martra, T. Cacciatori, L. Marchese, J.S.J. Hargreaves, I.M. Mellor, R.W. Joyner, S. Coluccia, Catal. Today 70 (2001) 121.
[27] G. Spoto, S. Bordiga, D. Scarano, A. Zecchina, Catal. Lett. 13 (1992) 39.
[28] G. Spoto, A. Zecchina, S. Bordiga, G. Ricchiardi, G. Martra, G. Leofanti, G. Petrini, Appl. Catal. B 3 (1994) 151.
[29] G. Spoto, S. Bordiga, G. Ricchiardi, D. Scarano, A. Zecchina, F. Geobaldo, J. Chem. Soc., Faraday Trans. 91 (1995) 3285.
[30] G. Spoto, E. Gribov, S. Bordiga, C. Lamberti, G. Ricchiardi, D. Scarano, A. Zecchina, Chem. Commun. (2004) 2768.
[31] C. Lamberti, S. Bordiga, M. Salvalaggio, G. Spoto, A. Zecchina, F. Geobaldo, G. Vlaic, M. Bellatreccia, J. Phys. Chem. B 101 (1997) 344.
[32] C. Lamberti, G.T. Palomino, S. Bordiga, G. Berlier, F. D'Acapito, A. Zecchina, Angew. Chem. Int. Edit. 39 (2000) 2138.
[33] C. Lamberti, S. Bordiga, F. Bonino, C. Prestipino, G. Berlier, L. Capello, F. D'Acapito, F.X.L.I. Xamena, A. Zecchina, Phys. Chem. Chem. Phys. 5 (2003) 4502.
[34] A. Zecchina, S. Bordiga, M. Salvalaggio, G. Spoto, D. Scarano, C. Lamberti, J. Catal. 173 (1998) 540.
[35] A. Zecchina, S. Bordiga, G.T. Palomino, D. Scarano, C. Lamberti, M. Salvalaggio, J. Phys. Chem. B 103 (1999) 3833.
[36] V. Bolis, S. Maggiorini, L. Meda, F. D'Acapito, G.T. Palomino, S. Bordiga, C. Lamberti, J. Chem. Phys. 113 (2000) 9248.
[37] V. Bolis, S. Bordiga, G.T. Palomino, A. Zecchina, C. Lamberti, Thermochim. Acta 379 (2001) 131.
[38] V. Bolis, A. Barbaglia, S. Bordiga, C. Lamberti, A. Zecchina, J. Phys. Chem. B 108 (2004) 9970.
[39] G. Turnes Palomino, S. Bordiga, A. Zecchina, G.L. Marra, C. Lamberti, J. Phys. Chem. B 104 (2000) 8641.
[40] C. Prestipino, G. Berlier, F.X. Llabrés i Xamena, G. Spoto, S. Bordiga, A. Zecchina, G.T. Palomino, T. Yamamoto, C. Lamberti, Chem. Phys. Lett. 363 (2002) 389.
[41] L. Rodriguez-Santiago, M. Sierka, V. Branchadell, M. Sodupe, J. Sauer, J. Am. Chem. Soc. 120 (1998) 1545.
[42] D. Nachtigallova, P. Nachtigall, M. Sierka, J. Sauer, Phys. Chem. Chem. Phys. 1 (1999) 2019.
[43] P. Nachtigall, D. Nachtigallova, J. Sauer, J. Phys. Chem. B 104 (2000) 1738.
[44] D. Nachtigallova, P. Nachtigall, J. Sauer, Phys. Chem. Chem. Phys. 3 (2001) 1552.
[45] G. Calzaferri, C. Leiggener, S. Glaus, D. Schurch, K. Kuge, Chem. Soc. Rev. 32 (2003) 29.
[46] O. Bludsky, M. Silhan, D. Nachtigallova, P. Nachtigall, J. Phys. Chem. A 107 (2003) 10381.
[47] M. Davidova, D. Nachtigallova, R. Bulanek, P. Nachtigall, J. Phys. Chem. B 107 (2003) 2327.
[48] M. Davidova, D. Nachtigallova, P. Nachtigall, J. Sauer, J. Phys. Chem. B 108 (2004) 13674.
[49] S.I. Zones, US Patent 4 544 538 (1985).
[50] S. Bordiga, L. Regli, D. Cocina, C. Lamberti, M. Bjørgen, K.P. Lillerud, J. Phys. Chem. B 109 (2005) 2779.
[51] A. Zecchina, S. Bordiga, J.G. Vitillo, G. Ricchiardi, C. Lamberti, G. Spoto, M. Bjørgen, K.P. Lillerud, J. Am. Chem. Soc. 127 (2005) 6361.
[52] E. Guglielminotti, S. Coluccia, E. Garrone, L. Cerruti, A. Zecchina, J. Chem. Soc., Faraday Trans. I 75 (1979) 96.
[53] S. Coluccia, M. Baricco, L. Marchese, G. Martra, A. Zecchina, Spectrochim. Acta A 49 (1993) 1289.
[54] S. Furuyama, H. Fujii, M. Kawamura, T. Morimoto, J. Phys. Chem. 82 (1978) 1028.
[55] E.A. Paukshtis, N.E. Yurchenko, Russ. Chem. Rev. 52 (1983) 426.
[56] M.I. Zaki, H. Knözinger, Spectrochim. Acta A 43 (1987) 1455.
[57] E. Knözinger, K.H. Jacob, P. Hofmann, J. Chem. Soc., Faraday Trans. 89 (1993) 1101.
[58] N.S. Hush, M.L. Williams, J. Mol. Spectrosc. 50 (1974) 349.
[59] G. Pacchioni, G. Cogliandro, P.S. Bagus, Int. J. Quant. Chem. 42 (1992) 1115.
[60] C. Lamberti, S. Bordiga, F. Geobaldo, A. Zecchina, C. Otero Areán, J. Chem. Phys. 103 (1995) 3158.
[61] A.G. Pelmenschikov, G. Morosi, A. Gamba, S. Coluccia, J. Phys. Chem. 99 (1995) 15018.

[62] E.A. Paukshtis, R.I. Soltanov, N.E. Yurchenko, React. Kinet. Catal. Lett. 16 (1981) 93.
[63] C. Otero Areán, O.V. Manoilova, B. Bonelli, M.R. Delgado, G.T. Palomino, E. Garrone, Chem. Phys. Lett. 370 (2003) 631.
[64] O. Dulaurent, D. Bianchi, Appl. Catal. A: Gen. 207 (2001) 211.
[65] D. Scarano, G. Spoto, S. Bordiga, S. Coluccia, A. Zecchina, J. Chem. Soc., Faraday Trans. 88 (1992) 291.
[66] S. Coluccia, L. Marchese, Catal. Today 41 (1998) 229.
[67] M.A. Babaeva, D.S. Bystrov, A.Y. Kovaligia, A.A. Tsyganenko, J. Catal. 123 (1990) 396.
[68] T. Ito, H. Kobayashi, T. Tashiro, Il Nuovo Cimento D 19 (1997) 1695.
[69] T. Tashiro, J. Ito, R.B. Sim, K. Miyazawa, E. Hamada, K. Toi, H. Kobayashi, T. Ito, J. Phys. Chem. 99 (1995) 6115.
[70] X. Lu, X. Xu, N.Q. Wang, Q.N. Zhang, J. Phys. Chem. B 104 (2000) 10024.
[71] L. Schlapbach, A. Züttel, Nature 414 (2001) 353.
[72] F.S. Stone, E. Garrone, A. Zecchina, Mater. Chem. Phys. 13 (1985) 331.
[73] O. Diwald, E. Knözinger, J. Phys. Chem. B 106 (2002) 3495.
[74] M. Sterrer, T. Berger, O. Diwald, E. Knözinger, J. Am. Chem. Soc. 125 (2003) 195.
[75] M. Chiesa, M.C. Paganini, E. Giamello, C. Di Valentin, G. Pacchioni, Angew. Chem. Int. Edit. 42 (2003) 1759.
[76] S. Coluccia, F. Boccuzzi, G. Ghiotti, C. Morterra, J. Chem. Soc., Faraday Trans. I 78 (1982) 2111.
[77] E. Garrone, F.S. Stone, J. Chem. Soc., Faraday Trans. I 83 (1987) 1237.
[78] D. Ricci, C. Di Valentin, G. Pacchioni, P.V. Sushko, A.L. Shluger, E. Giamello, J. Am. Chem. Soc. 125 (2003) 738.
[79] E.N. Gribov, S. Bertarione, D. Scarano, C. Lamberti, G. Spoto, A. Zecchina, J. Phys. Chem. B 108 (2004) 16174.
[80] S. Bordiga, E. Garrone, C. Lamberti, A. Zecchina, C. Otero Arean, V.B. Kazansky, L.M. Kustov, J. Chem. Soc., Faraday Trans. 90 (1994) 3367.
[81] J. Heidberg, N. Gushanskaya, O. Schönekäs, R. Schwarte, Surf. Sci. 331–333 (1995) 1473.
[82] M. Sigl, S. Ernst, J. Weitkamp, H. Knözinger, Catal. Lett. 45 (1997) 27.
[83] S. Briquez, S. Picaud, C. Girardet, P.N.M. Hoang, J. Heidberg, A. Vossberg, J. Chem. Phys. 109 (1998) 6435.
[84] V.B. Kazansky, V.Y. Borovkov, A. Serich, H.G. Karge, Micropor. Mesopor. Mater. 22 (1998) 251.
[85] V.B. Kazansky, F.C. Jentoft, H.G. Karge, J. Chem. Soc., Faraday Trans. 94 (1998) 1347.
[86] F. Stephanie-Victoire, A.M. Goulay, E. Cohen de Lara, Langmuir 14 (1998) 7255.
[87] F. Stephanie-Victoire, E. Cohen de Lara, J. Chem. Phys. 109 (1998) 6469.
[88] A. Zecchina, C.O. Arean, G.T. Palomino, F. Geobaldo, C. Lamberti, G. Spoto, S. Bordiga, Phys. Chem. Chem. Phys. 1 (1999) 1649.
[89] V.B. Kazansky, J. Mol. Catal. A: Chem. 141 (1999) 83.
[90] J. Heidberg, A. Vossberg, M. Hustedt, M. Thomas, S. Briquez, S. Picaud, C. Girardet, J. Chem. Phys. 110 (1999) 2566.
[91] L. Regli, A. Zecchina, J.G. Vitillo, D. Cocina, G. Spoto, C. Lamberti, K.P. Lillerud, U. Olsbye, S. Bordiga, Phys. Chem. Chem. Phys. 7 (2005) 3197.
[92] M. Iwamoto, H. Furukawa, Y. Mine, F. Uemura, S. Mikuriya, S. Kagawa, J. Chem. Soc., Chem. Commun. (1986) 1272.
[93] X. Solans-Monfort, V. Branchadell, M. Sodupe, C.M. Zicovich-Wilson, E. Gribov, G. Spoto, C. Busco, P. Ugliengo, J. Phys. Chem. B 108 (2004) 8278.
[94] A.I. Serykh, V.B. Kazansky, Phys. Chem. Chem. Phys. 6 (2004) 5250.
[95] H.S. Plitt, M.R. Bar, R. Ahlrichs, H. Schnockel, Angew. Chem. Int. Edit. Engl. 30 (1991) 832.
[96] Y. Kuroda, Y. Yoshikawa, R. Kumashiro, M. Nagao, J. Phys. Chem. B 101 (1997) 6497.
[97] P.R. Kemper, P. Weis, M.T. Bowers, P. Maitre, J. Am. Chem. Soc. 120 (1998) 13494.
[98] J.A. Rabo, R.J. Pellet, P.K. Coughlin, E.S. Shamson, in: H.G. Karge, J. Weitkamp (Eds.), Zeolites as Catalysts and Detergent Builders, Elsevier, Amsterdam, 1989, p. 1.
[99] J. Chen, P.A. Wright, S. Natarajan, J.M. Thomas, Stud. Surf. Sci. Catal. 84 (1994) 1731.
[100] M. Stöcker, Micropor. Mesopor. Mater. 29 (1999) 3.
[101] J.F. Haw, W. Song, D.M. Marcus, J.B. Nicholas, Acc. Chem. Res. 36 (2003) 317.
[102] L.J. Smith, A. Davidson, A.K. Cheetham, Catal. Lett. 49 (1997) 143.
[103] L.J. Smith, A.K. Cheetham, L. Marchese, J.M. Thomas, P.A. Wright, J. Chen, E. Gianotti, Catal. Lett. 41 (1996) 13.
[104] S. Bordiga, L. Regli, C. Lamberti, A. Zecchina, M. Bjørgen, K.P. Lillerud, J. Phys. Chem. B 109 (2005) 7724.
[105] E. Garrone, C. Otero Areán, Chem. Soc. Rev. 34 (2005) 846.
[106] A. Zecchina, G. Spoto, S. Bordiga, Phys. Chem. Chem. Phys. 7 (2005) 1627.